Step-by-Step Growth of HKUST-1 on Functionalized TiO$_2$ Surface: An Efficient Material for CO$_2$ Capture and Solar Photoreduction

Barbara Di Credico [1],*, Matteo Redaelli [1], Marianna Bellardita [2] , Massimo Calamante [3], Cinzia Cepek [4], Elkid Cobani [1], Massimiliano D'Arienzo [1], Claudio Evangelisti [5] , Marcello Marelli [5] , Massimo Moret [1], Leonardo Palmisano [2] and Roberto Scotti [1]

[1] Department of Materials Science, INSTM, University of Milano-Bicocca, Via R. Cozzi, 55, 20125 Milano, Italy; mat.redaelli@gmail.com (M.R.); e.cobani@campus.unimib.it (E.C.); massimiliano.darienzo@unimib.it (M.D.); massimo.moret@unimib.it (M.M.); roberto.scotti@unimib.it (R.S.)

[2] Dipartimento di Energia, Ingegneria dell'Informazione e Modelli Matematici DEIM—Università degli Studi di Palermo, Viale delle Scienze (Ed. 6), 90128 Palermo, Italy; marianna.bellardita@unipa.it (M.B.); leonardo.palmisano@unipa.it (L.P.)

[3] Istituto di Chimica dei Composti Organometallici ICCOM-CNR, Via Madonna del Piano, 10, 50019 Sesto Fiorentino (Firenze), Italy; mcalamante@iccom.cnr.it

[4] Istituto Officina dei Materiali IOM-CNR, Laboratorio TASC, Area Science Park-Basovizza, Edificio MM, Strada Statale 14, km 163,5, I-34149 Trieste, Italy; cepek@iom.cnr.it

[5] Istituto di Scienze e Tecnologie Molecolari ISTM-CNR, via G. Fantoli, 16-15, 20138 Milano, Italy; claudio.evangelisti@istm.cnr.it (C.E.); m.marelli@istm.cnr.it (M.M.)

* Correspondence: barbara.dicredico@unimib.it; Tel.: +39-02-64485023

✓ check for updates

Abstract: The present study reports on a simple preparation strategy of a hybrid catalyst, TiO$_2$/HKUST-1, containing TiO$_2$ anatase nanoparticles (NPs) with tailored morphology and photocatalytic activity coupled with a porous metal-organic framework (MOF), namely HKUST-1, as an advanced material for the CO$_2$ photocatalytic reduction. In detail, TiO$_2$/HKUST-1 catalyst was prepared via an easy slow-diffusion method combined with a step-by-step self-assembly at room temperature. The growth of crystalline HKUST-1 onto titania surface was achieved by functionalizing TiO$_2$ nanocrystals, with phosphoesanoic acid (PHA), namely TiO$_2$-PHA, which provides an intimate contact between MOF and TiO$_2$. The presence of a crystalline and porous shell of HKUST-1 on the TiO$_2$ surfaces was assessed by a combination of analytical and spectroscopic techniques. TiO$_2$/HKUST-1 nanocomposite showed a significant efficiency in reducing CO$_2$ to CH$_4$ under solar light irradiation, much higher than those of the single components. The role of MOF to improve the photoreduction process under visible light was evidenced and attributed either to the relevant amount of CO$_2$ captured into the HKUST-1 porous architecture or to the hybrid structure of the material, which affords enhanced visible light absorption and allows an effective electron injection from TiO$_2$-PHA to HKUST-1, responsible for the photochemical reduction of CO$_2$.

Keywords: CO$_2$ photoreduction; metal-organic frameworks; HKUST-1; titanium dioxide; hybrid nanocomposite

1. Introduction

The significant increase in the CO$_2$ level in the past several decades is a matter of great concern [1,2]. While there are considerable investments in developing methods to reduce CO$_2$ emissions, it is apparent that its atmospheric concentration will continue to monotonically

increase for the foreseeable future, due to fossil fuel and industry consumption, land-use changes, such as deforestation and fires, and so on [3–5]. Suggestions have been made to sequester carbon dioxide, such as sorption into new functional materials [6]. However, the possibility to recycle CO_2 via conversion into high-energy content fuels appears an attractive option, but the process is energy demanding and useful only if a renewable energy source can be used. A possible sustainable approach lies in the TiO_2-assisted photocatalytic reduction of CO_2 to renewable fuels (i.e., CO, CH_3OH, HCOOH, CH_4) using solar light as photon source [7–9].

Although TiO_2 has been demonstrated to be a promising photocatalyst for CO_2 reduction [10–13], its activity is limited owing to the poor adsorption capability, the low quantum yield and solar energy conversion efficiency. Hence, the combination of TiO_2 with materials with remarkable adsorption capacity, like zeolites or other mesoporous materials [14–16] has been found to be a promising method for enhancing its photocatalytic performance. Besides, many efforts have been devoted to extending the light absorption of TiO_2 to the visible region, but the activation of the TiO_2 photocatalytic response in the visible region still remains a challenge.

To overcome these issues, several recent studies support the idea of using Metal Organic Frameworks (MOF) as porous coating of TiO_2 [17]. MOFs materials, made by assembling metal ions with organic ligands as linkers, possess exceptionally high pore volume and surface area, due to uniform and continuous structural cavities, and different active sites on the pores surface [18,19]. These characteristics depend both on the kind of metal and linker, and provide cage-like cavities with tunable properties, such as charge, polarity, redox potential, hydrophobicity/hydrophilicity, and aromatic/lipophilic character [20,21]. In addition, it is important to point out that MOFs could act also as a photosensitizer of TiO_2, extending its absorption toward the visible range and inhibiting the electron-hole recombination process, thanks to the charge transfer process between semiconductor and MOF [22–25].

In the last decade, some examples of TiO_2 hybrid systems containing Zr [26], Fe [27], Al [28], Cd [29], Cu [30], based MOFs have been reported to reduce CO_2 mainly to CO, formate and methane. In any case, the interfacial interaction between TiO_2 and MOFs was identified as the crucial point for the improved photocatalytic conversion [23,24].

Among MOFs, a copper-based one, $[Cu_3(BTC)_2(H_2O)_3]_n$, (BTC = benzene-1,3,5-tricarboxylate), namely HKUST-1 [31], has been recognized as an excellent material for CO_2 storage [32,33] due to the presence of unsaturated metal sites, available for interaction with CO_2, H_2 and other gases [34,35]. However, only a few TiO_2 materials containing HKUST-1 for CO_2 photoreduction have been reported so far [36,37]. Li et al. synthesized a HKUST/TiO_2 core/shell structure by coating a nanocrystalline TiO_2 shell onto the HKUST-1 core, with HKUST-1/TiO_2 ratio of 0.5 [36]. This MOF/semiconductor material was able to convert CO_2 into CH_4 under UV illumination with improved performance compared to bare TiO_2. The authors concluded that in HKUST/TiO_2, UV photogenerated electrons can be effectively transferred from TiO_2 to the MOF, avoiding charge recombination, and, in turn, to the gas molecules adsorbed by the porous structure. However, the suggested electron transfer was correlated to the photocatalytic reduction performed exclusively under UV irradiation.

Recently, He and coworkers [37] reported the synthesis of TiO_2 embedded in the HKUST-1 matrix via a rapid aerosol route with HKUST-1/TiO_2 ratio of 3.33. This significantly improves the CO_2 photoreduction to CO, in comparison with pristine TiO_2. The enhanced performance was attributed only to the enhanced reactant adsorption on the catalyst due to MOF presence, even if no electron transfer processes were highlighted.

Despite the promising performance of the abovementioned hybrid TiO_2-MOF catalysts, several critical points should be still clarified in order to define the activation role of MOF in the CO_2 photoreduction, specifically under visible light.

In this context, we report a simple synthesis of porous hybrid catalyst, based on HKUST-1 anchored to anatase TiO_2 nanoparticles (NPs) with controlled rhombic elongated (RE) morphology, by means of a phosphonic acid as coupling agent. TiO_2 NPs were chosen for their photoactivity [38],

while HKUST-1 for its ability in favoring high CO_2 adsorption as well as controlled release kinetics [39], so that MOF pores may behave like "nano-reactors", in which the substrate is confined near to the TiO_2 surface.

In detail, we have prepared, by a cheap and easy to scale-up soft-chemistry method, TiO_2 nanocrystals having tailored structural and morphological features, with exposed {101} and {010} facets which are known to be active in photo-reduction reactions [40,41]. TiO_2 NPs were functionalized with an asymmetric organic linker, namely 6-phosphohexanoic acid (PHA), suitable to covalently interact with the oxide surface by Ti-O-P bond, as well as to selectively bind copper metal ions by carboxylate functionality. The growth of HKUST-1 on PHA-modified TiO_2 NPs (TiO_2-PHA) was obtained using a slow-diffusion method combined with a step-by-step self-assembly approach [42]. After complexation of Cu^{2+} metal ions by the carboxylic groups, the metal-carboxylate centers react with the BTC ligand activating the crystalline growth of the HKUST-1 structure on the oxide surface.

This synthetic strategy, based on the TiO_2 functionalization with an organic linker, greatly (i) facilitates NPs dispersion, preventing undesirable agglomeration phenomena, (ii) promotes the crystalline growth of MOF layers on TiO_2 surface and (iii) favors an intimate contact between TiO_2 and MOF, which makes easier, in principle, the electron transfer at the hybrid interface.

TiO_2/HKUST-1 nanocomposite was characterized by a combination of analytical and spectroscopic techniques. After determining the structural and morphological features, the CO_2 adsorption aptitude and the photocatalytic performances of the developed hybrid material were examined. CO_2 photoreduction tests were performed under sunlight, in ambient conditions and in a heterogeneous gas/solid set-up, in order to simulate the conditions under which CO_2 capture and fixation proceed in a single step, while most of the existent studies describe gas/liquid systems. Based on the photocatalytic results, a model for explaining the possible charge transfer between HKUST-1 and TiO_2-PHA in TiO_2/HKUST-1 have been proposed, in connection with the peculiar structure and morphology of hybrid material.

2. Results and Discussion

TiO_2/HKUST-1 catalyst was prepared via a simple slow-diffusion method combined with a step-by-step self-assembly at room temperature. Firstly, the solvothermal synthesis of shape-controlled anatase nanocrystals was performed according to a previously reported procedure [43] (Scheme 1, STEP 1) by reaction of the titanium (IV) butoxide (TB), in the presence of oleic acid (OA) and oleylamine (OM). After removing the residual amounts of capping agents by using tetramethylammonium hydroxide (TMAH) [44] (STEP 2), the pre-synthetized TiO_2 NPs have been functionalized with PHA (STEP 3), able to covalently interact with the oxide surface by the phosphonic group, as well as to bind copper metal ions by carboxylic acid, promoting the grown of HKUST-1.
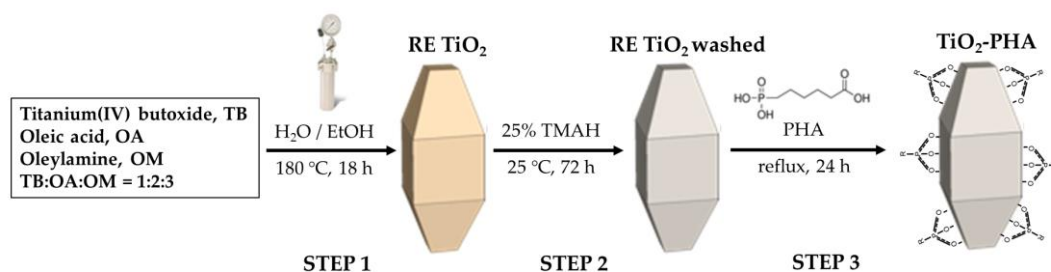
Scheme 1. Schematic synthesis of TiO_2 nanoparticles (NPs) with controlled rhombic elongated (RE) morphology (STEP 1 and 2) and functionalization with 6-phosphohexanoic acid (PHA) of TiO_2 NPs (TiO_2-PHA, STEP 3).

After that, TiO_2/HKUST-1 was prepared by a step-by-step *self-assembly* at low temperature (40 °C) (Scheme 2). In detail, the copper centers of the copper acetate (AcCu(II)) can interact with the carboxyl groups of TiO_2-PHA and react with the carboxyl groups of H_3BTC ligands.
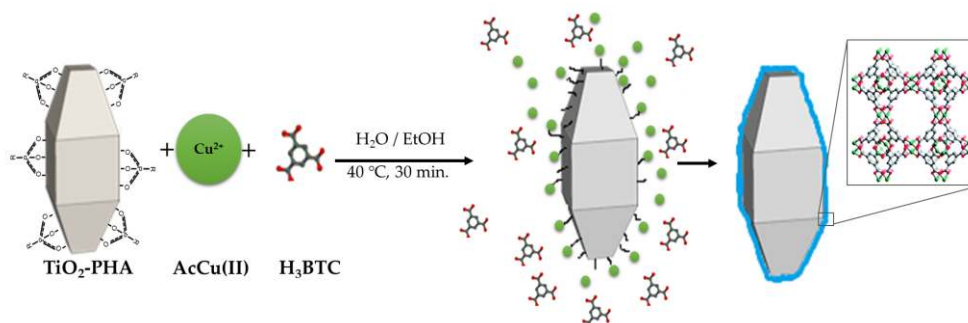
Scheme 2. Synthesis of the TiO_2/HKUST-1 by using TiO_2-PHA, benzene-1,3,5-tricarboxylic acid (H_3BTC) and copper acetate (AcCu(II) as starting materials. Green, gray, and red spheres represent Cu, C, and O atoms, respectively; H atoms have been omitted for clarity. The sky-blue line represents HKUST-1 shells onto TiO_2-PHA.

2.1. Spectroscopic and Morphological Characterization of TiO_2-PHA and TiO_2/HKUST-1

The characterization of TiO_2-PHA and TiO_2/HKUST-1 was performed in order to demonstrate: (i) the effective functionalization of TiO_2 NPs by PHA phosphonic groups and consequently (ii) the crystalline growth of the HKUST-1 structure on the oxide surface.

The crystal structure of the materials was checked by powder X-ray diffraction (PXRD) analysis (Figure 1). PXRD patterns of TiO_2/HKUST-1 sample (Figure 1a) showed the superimposed pattern of HKUST-1 (Figure 1c) [31] and anatase TiO_2 diffraction peaks [45] (Figure 1b), corresponding to (101), (004), (200), (105), and (211) reflections highlighted in the figure. In particular, the pattern indicates that HKUST-1 shells in TiO_2/HKUST-1 are highly crystalline, as confirmed by transmission electron microscopy (TEM), while pure HKUST-1 contains a greater fraction of amorphous phase.

This suggests that both TiO_2 NPs functionalization with specific carboxylate end-group of PHA and the use of step-by-step self-assembly synthesis promote the crystalline growth of MOF porous material, even under mild conditions. In detail, in the first step of HKUST-1 synthesis, PHA carboxylic groups allow the complexation of Cu^{2+} metal ions anchoring them onto the oxide surface. In the second step, the copper centres covalently bond to the BTC ligands enabling the growing of HKUST-1 on the TiO_2 surface and the control of its crystallographic orientations [46].

The observed HKUST-1 crystallinity represents a key feature to impart desired functionality to the final hybrid material, such as improved adsorption ability and consequent enhanced catalytic activity [47].

Attenuated Total Reflection Fourier Transform Infrared Spectroscopy (ATR-FTIR) spectroscopy was performed in order to investigate the TiO_2–MOF hybrid catalyst (Figure 2).

Specifically, the spectrum of PHA shows the following main bands (Figure 2a, grey line): the intense carboxyl stretching vibration at 1710 cm^{-1}; the P=O stretching vibration at 1220 cm^{-1} and the methylene C–H bending at 1309 and 1213 cm^{-1} (very weak).

After titania functionalization, the spectrum of TiO_2-PHA (Figure 2a,b, red line) still displays the characteristic absorption bands at 1715 cm^{-1} deriving from COOH of the PHA, instead the PHA band at 1220 cm^{-1}, attributed to the P=O stretching vibration, disappears (red line in Figure 2b). TiO_2-PHA spectrum also shows the vibrations at 995 cm^{-1} and at 1150 cm^{-1}, attributable to the symmetric stretching of P-O-Ti and P-CH$_2$ bonds, respectively [48]. These results suggest that phosphoryl groups of PHA interact with TiO_2 surfaces.
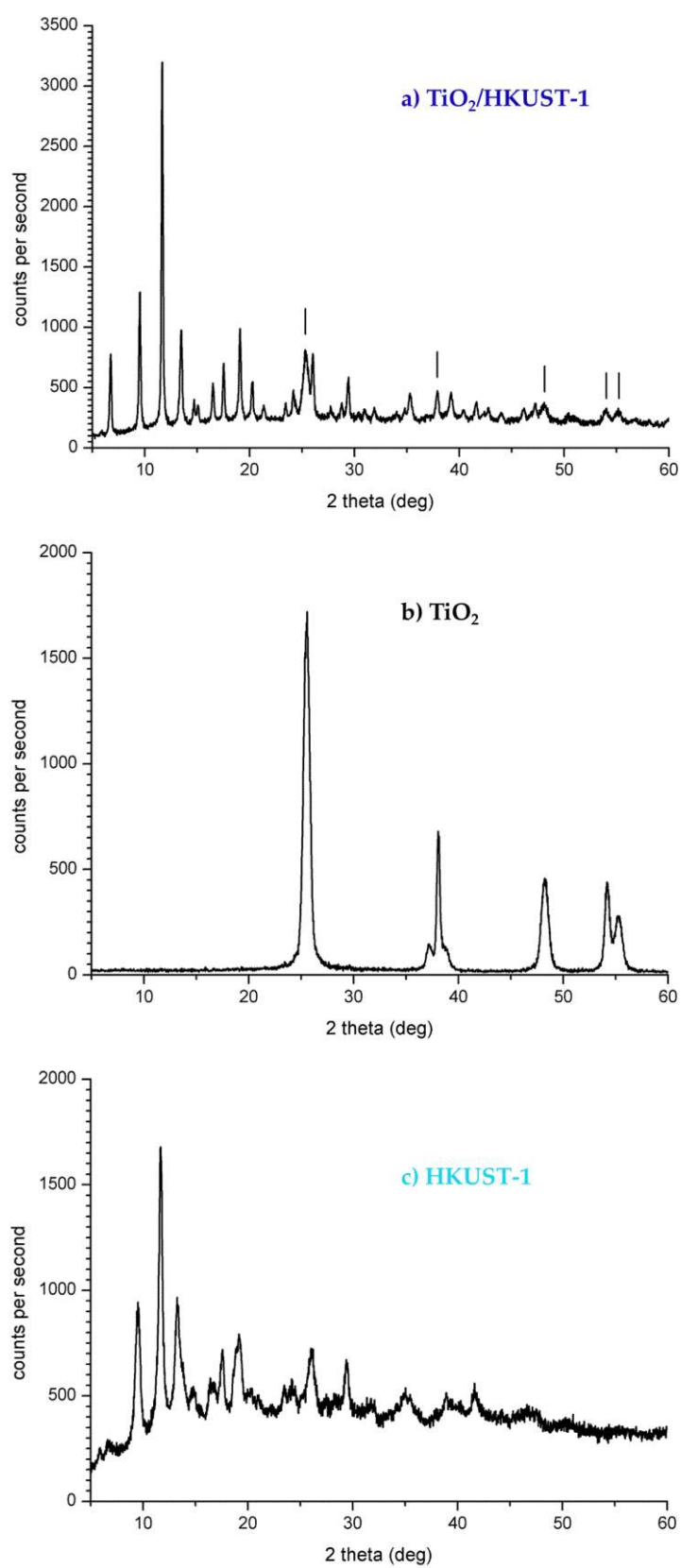
Figure 1. Powder X-ray diffraction (PXRD) pattern of (**a**) TiO$_2$/HKUST-1 (overhanging bars correspond to the most intense diffraction peaks of anatase TiO$_2$), (**b**) TiO$_2$ and (**c**) HKUST-1.
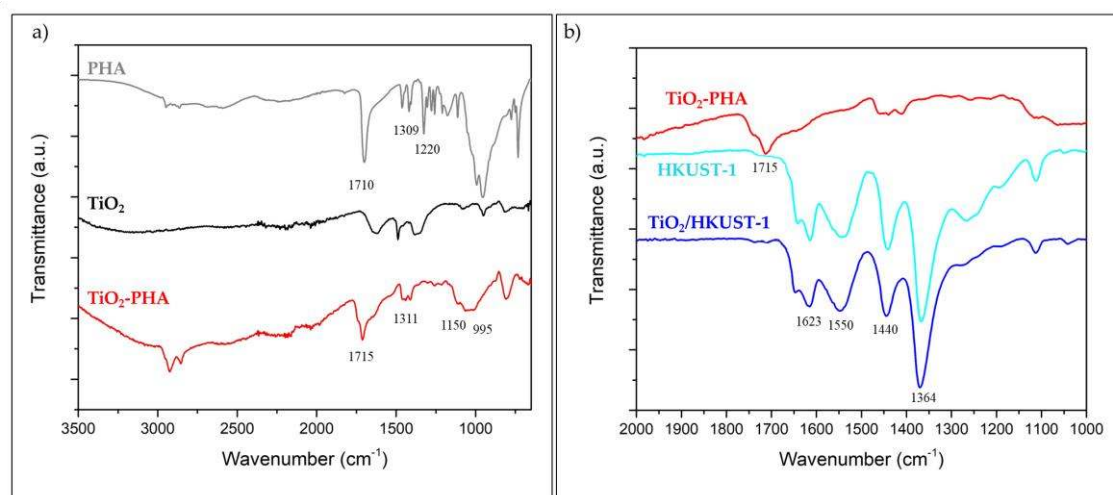
Figure 2. FTIR spectra of: (**a**) pristine PHA (top, gray line), RE TiO_2 NPs (black line) and TiO_2-PHA (red line) and (**b**) TiO_2-PHA (red line), HKUST-1 (sky blue line) and TiO_2/HKUST-1 (blue line) in the 2000–1000 cm^{-1} range.

The spectra of TiO_2/HKUST-1 (Figure 2b, blue line) and pure HKUST-1 (Figure 2b, sky blue line) look rather similar and show characteristics analogous to those reported in the literature [49]. The bands at 1623 and 1550 cm^{-1} and at 1440 and 1364 cm^{-1}, corresponding to the asymmetric and symmetric stretching vibrations of the BTC carboxylate groups, confirm that MOF coating TiO_2 in the composite maintains the structural features of HKUST-1.

In addition, the band centred at 1715 cm^{-1}, corresponding to the carbonyl stretching in pure TiO_2-PHA, shifts to lower energy in the TiO_2/HKUST-1 spectrum, evidencing between 1540 and 1650 cm^{-1} the antisymmetric mode of the chelated carboxyl group. This supports the deprotonation of carboxylic acid group and coordination with copper, confirming the effective role of PHA as grafting group for HKUST-1.

The thermal behavior of the hybrid material was assessed by thermogravimetric analysis (TGA). Figure 3 shows TGA curves obtained for both as-prepared shape-controlled TiO_2 (black line) and TiO_2-PHA (red line) nanocrystals. In the as-prepared sample (black curve), a small weight loss (~3%) beginning at nearly 30 °C and continuing until 250 °C is detectable, which can be ascribed to physisorbed solvents removal. A more relevant weight loss is observable instead in TiO_2-PHA in a wide temperature range, from 230 to 400 °C, attributable to the thermal degradation of the PHA. The total amount of PHA grafted onto TiO_2 (11.2 wt. %) was evaluated by the net weight loss of TiO_2–PHA between 150 and 400 °C, i.e., considering the total weight loss with exclusion of that associated to TiO_2 (i.e., 3 wt. %).

TGA analysis was also performed on TiO_2/HKUST-1 (blue line), in order to determine the real amount of HKUST-1 in the hybrid material. The loading of HKUST-1 (73% wt. %) was estimated from the net weight loss of TiO_2/HKUST-1 between 150 and 400 °C, i.e., considering the total weight loss with the exclusion of that associated to pure PHA.

The morphological features of both TiO_2 NPs and hybrid TiO_2/HKUST-1 materials were investigated by TEM microscopy.

RE TiO_2 sample exhibits well-formed rhombic elongated nanocrystals with estimated size of 16.5 nm in width and 45–60 nm in length (Table S1 in Supplementary Materials), and with mainly exposed {101} and {010} crystal facets (Figure 4a,b), according to the results reported by Dihn et al. [50].

In TiO_2/HKUST-1 hybrid composite (Figure 4c,d), TiO_2 NPs maintain their peculiar anisotropic morphology and appear organized in nanometric aggregates (Figure 4c). At a higher magnification (Figure 4d), the presence of HKUST-1 shells uniformly grown onto the TiO_2 surfaces and intimately connecting the NPs can be observed (yellow arrows in d). The uniform distribution of HKUST-1 around

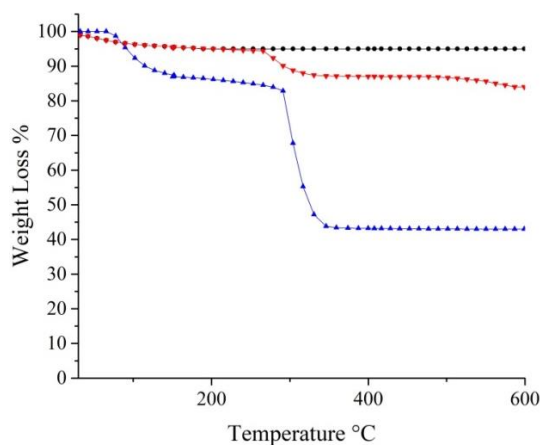TiO$_2$ crystals into the hybrid material is also relevant; this is expected from the use of functionalized TiO$_2$ NPs.

Figure 3. TGA curves of RE TiO$_2$ NPs (black line), TiO$_2$-PHA (red line), and TiO$_2$/HKUST-1 (blue line).

Selected area electron diffraction (SAED) analysis was in agreement with XRD and high-resolution TEM (HRTEM) data, confirming again the presence of TiO$_2$ anatase phase in both TiO$_2$-PHA and TiO$_2$/HKUST-1 samples and of crystalline HKUST-1 in the hybrid system, as revealed by lattice fringes analysis (Figure S1). Finally, STEM-EDS analysis reveal the presence of Ti and Cu with a ratio close to the theoretical 1:1 (Figure S2).

In summary, TEM investigation indicates the successful formation of the hybrid structure and supports close interaction between the RE NPs and HKUST-1.
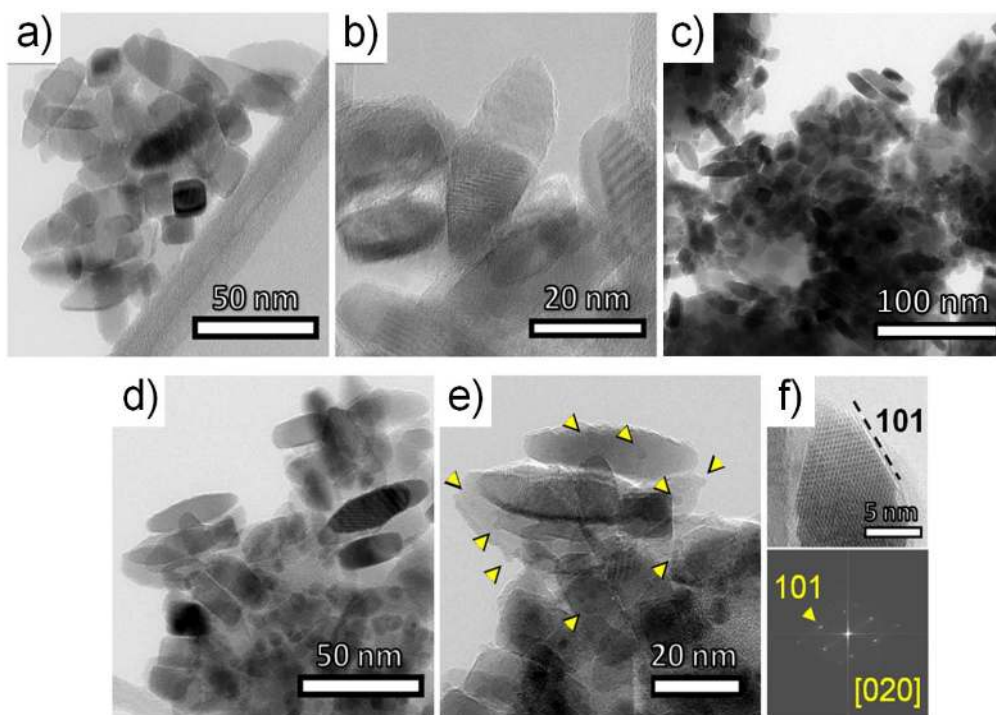

Figure 4. HRTEM images of (**a**,**b**) shape-controlled RE TiO$_2$ anatase NPs; (**c**–**f**) TiO$_2$/HKUST-1 hybrid material. Yellow arrows in (**e**) highlight the close interaction between the two materials. Below the image (**f**) corresponding to Fast Fourier Transformation (FFT) of RE TiO$_2$.

As mentioned above, the coupling of HKUST-1 to TiO_2 NPs was aimed at: (i) favouring the CO_2 access to the catalytic sites by improving the porosity necessary to capture CO_2; (ii) activating TiO_2 photocatalytic response in the visible region.

Hence, the porosity of the TiO_2/HKUST-1 material was evaluated by nitrogen adsorption-desorption isotherms at 77 K (Figure 5a). The product exhibits a type IV isotherm with H1 hysteresis, which is typical of ordered mesoporous materials with uniform cylindrical pores [51]. The BET surface area resulted 349 m^2/g and the BJH pore-size distribution (Harkins–Jura approximation) shows the presence of mesopores with pore widths ca. 4 nm. The total pores volume corresponds to 0.25 cm^3/g. The specific surface area and total pore volumes of the bare TiO_2 NPs resulted instead 170 m^2/g and 0.21 cm^3/g respectively (Table S1).

In addition to a high specific surface area, TiO_2/HKUST-1 also showed a significant adsorption CO_2 capacity at room temperature (303 K) and atmospheric pressure (Figure 5b), reaching a percentage of CO_2 adsorbed of 10.16 wt. % (2.3 mmol/g). As expected, this amount is about three times lower than that reported for unsupported HKUST-1 under the same conditions (7.23 mmol/g) [52]. However, the CO_2 uptake is rather similar to that determined for other Cu-based MOFs with even higher BET surface area [53–55].
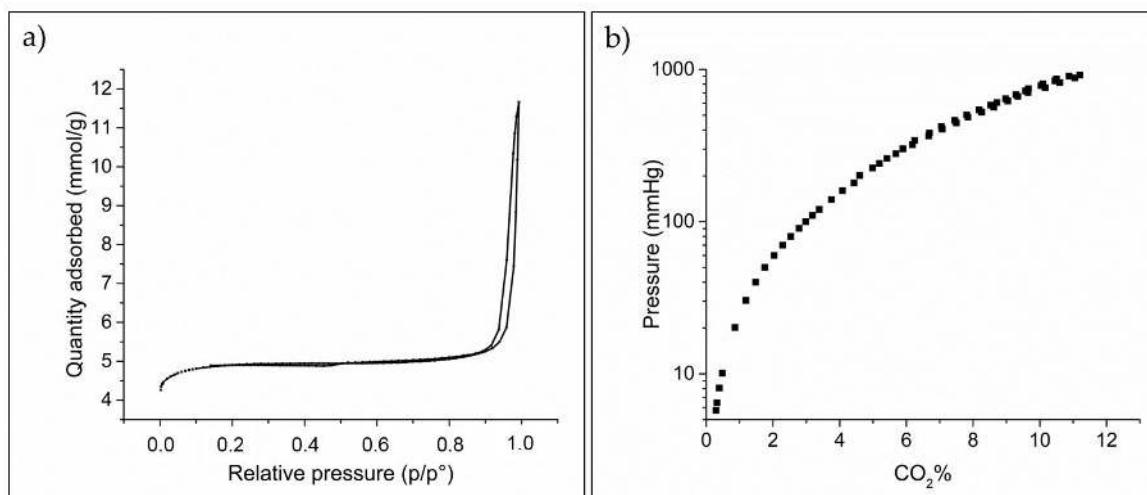

Figure 5. (**a**) N_2 adsorption isotherm of TiO_2/HKUST-1 at T = 77 K; (**b**) Pressure–composition plot for CO_2 physisorption on TiO_2/HKUST-1 at T = 303 K.

The diffuse reflectance ultraviolet-visible (DR-UV/Vis) spectra (Figure 6) were acquired for pure HKUST-1, TiO_2-PHA and TiO_2/HKUST-1, in order to study their optical absorption properties.

As expected, TiO_2-PHA (red line) absorbs mainly UV light while HKUST-1 (sky blue line) absorption extends over the visible range [49]. Notably, TiO_2/HKUST-1 (blue line) composite also shows a red shift of the optical absorption toward the visible range compared to TiO_2-PHA.

Based on the reflectance spectra (Figure S3), the band gap (E_g) of the samples (absorption edge in the case of nanocomposites) was determined by plotting the modified Kubelka-Munk function, $[F(R_\infty')h\nu]^{1/2}$, versus the energy of the excitation light. The calculated values of the TiO_2-PHA, HKUST-1 and TiO_2/HKUST-1 powders resulted 3.15 eV, 2.70 eV and 2.90 eV, respectively.

The enhanced absorption in the visible range of TiO_2/HKUST-1 compared to TiO_2, along with the smaller absorption edge value, provides a suitable platform for sensitizing TiO_2, making the obtained hybrid material an active catalyst under solar light.

In order to understand the electronic changes responsible for the absorption modification, the TiO_2/HKUST-1, TiO_2-PHA, and pristine TiO_2 and HKUST-1 samples were investigated X-ray photoelectron spectroscopy (XPS).

The survey spectra of TiO$_2$/HKUST-1 confirmed the presence of Cu, Ti, O, and C elements (Figure S4). The evolution of the Cu 2p, Ti 2p and O 1s core levels by XPS spectra (Figure 7 and Figure S5) allowed us to reveal the electronic structure of these levels in TiO$_2$/HKUST-1.
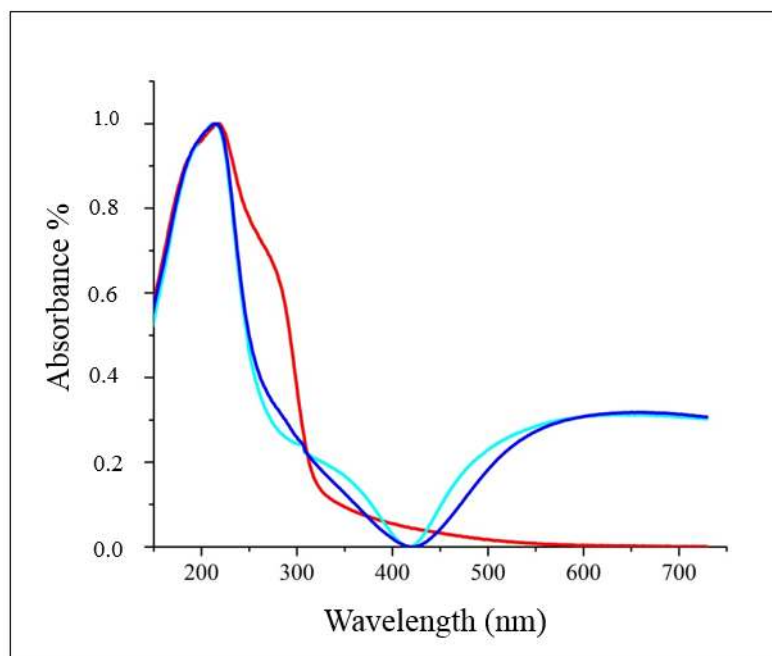

Figure 6. DR-UV-Vis spectra of TiO$_2$-PHA (red line), pure HKUST-1 (sky blue line) and TiO$_2$/HKUST-1 (blue line).
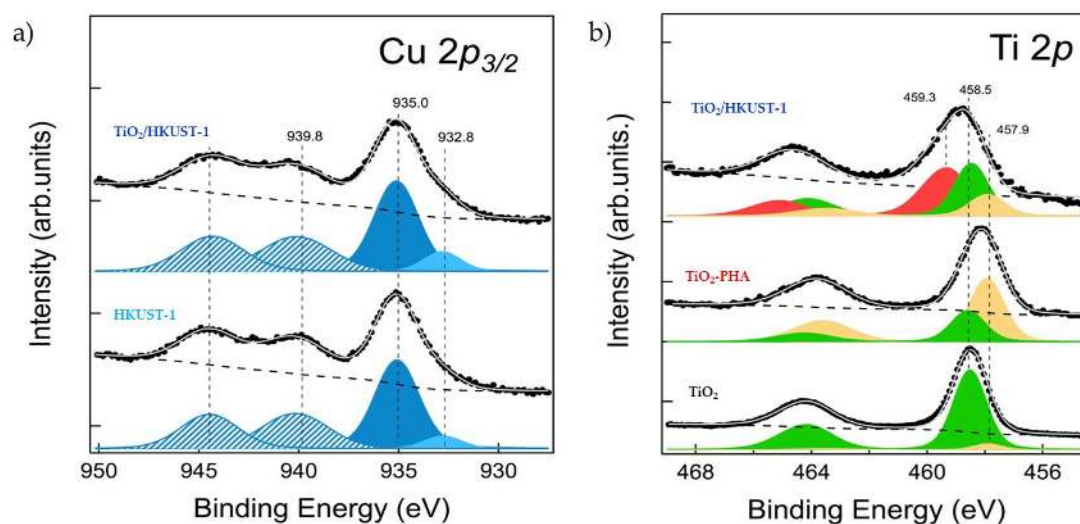

Figure 7. XPS spectra of (**a**) Cu 2$p_{3/2}$ in bare HKUST-1 and TiO$_2$/HKUST-1 [experimental data (dotted line), Cu(I) (sky blue peak), Cu(II) (blue peak) and its satellites (striped peaks)]; (**b**) Ti 2p in bare TiO$_2$, TiO$_2$-PHA and TiO$_2$/HKUST-1 [experimental data (dotted line), Ti(IV) (green and red peak), Ti(III) (yellow peak)].

The Cu $2p_{3/2}$ XPS spectra of HKUST-1 and TiO_2/HKUST-1 (Figure 7a) show peaks with similar lineshapes, suggesting that the copper chemical environment in the hybrid material is analogous to that of pristine HKUST-1. The main peak of Cu $2p_{3/2}$ was observed at 935.0 eV and it was deconvoluted into two components at 935.0 eV and 932.8 eV, originating from Cu(II) (blue peak in Figure 7a) and Cu(I) (sky blue peak in Figure 7a). By supposing a homogeneous stoichiometry, XPS indicates that Cu(I) percentage with respect to the total copper amount is ~11% in HKUST-1. This amount increases up to 17% in the final hybrid material [56].

The Ti $2p$ core level spectra of TiO_2, TiO_2-PHA and TiO_2/HKUST-1 samples are shown in Figure 7b. The Ti $2p_{3/2}$ binding energy (BE) of pure TiO_2 sample was found at 458.5 eV, corresponding to the Ti(IV) state (green peak in Figure 7b), with a small fraction of reduced Ti(III) at 457.9 (yellow peak in Figure 7b) [57], indicating the presence of Ti(III) defects originated during the solvothermal synthesis.

The Ti $2p_{3/2}$ level of TiO_2-PHA presents a broader line shape (458.2 eV) compared to pure TiO_2, indicating a higher amount of Ti(III) defects possibly generated after TiO_2 functionalization with PHA. It is well known that the concentration of Ti(III) strongly depends on the chemistry at the TiO_2 surface [58], where the presence of capping molecules, such as carboxylic or phosphonic acid [59,60], may cause the atomic oxygen diffusion, away from the lattice sites, reducing Ti(IV) to Ti(III) at the vacancy sites. This suggest that in TiO_2-PHA, phosphoesanoic acid induces a higher amount of Ti(III) sites at the TiO_2 surface, as confirmed by XPS analysis (Figure 7b).

In the case of TiO_2/HKUST-1, the Ti $2p$ peaks become even broader and shifts to higher BE compared to TiO_2-PHA. The fitting of the major band indicates the presence of three different components: Ti(IV) (green peak), Ti(III) species (yellow peak) and an additional Ti(IV) $2p$ peak at 459.3 eV (red peak). The appearance of additional Ti(IV) centers and the increase of Cu(I) atomic percentage in the final hybrid material (Figure 7a) suggests a partial oxidation of the Ti(III) species of TiO_2-PHA by the Cu(II) centers of HKUST-1. This hypothesis envisages the existence of an electron transfer between TiO_2 and HKUST-1 favoured by the intimate contact between titania and MOF anchored on its surface.

2.2. Photocatalytic Activity

The photocatalytic activity of TiO_2/HKUST-1 was evaluated in the CO_2 degradation. In accordance with previous studies reporting the gas phase CO_2 photoreduction [61–64], the main products were CH_4 and traces of CO [65–68]. We assume the detected hydrocarbons are unambiguously formed from CO_2 as carbon source, since the photocatalytic processes were performed after a peculiar cleaning procedure, in accordance with Mei et al. [69].

CO_2 photoreduction in the presence of TiO_2-PHA NPs (Table S2) produced a very low concentration of CH_4, equal to 0.69 μM (corresponding to 0.28 μmol g^{-1}) after 6 h of irradiation. The tests performed in the presence of bare HKUST-1 sample (Table S3) yielded also very low amounts of CH_4 (0.42 μmol g^{-1}). In the presence of TiO_2/HKUST-1 hybrid material, a significant generation of CH_4 was observed (Table S4), indicating that methane derived from CO_2 reduction and the catalytic ability of TiO_2/HKUST-1 is by the photocatalytic process affected during photocatalysis. A total amount of 2.63 μM CH_4, corresponding to 1.05 μmol g^{-1}, was produced after 6 h of irradiation without any significant morphological and structural changes of TiO_2/HKUST-1 (see Figure S6) after the second photocatalytic run.

As H_2 could be obtained as by-product during the CO_2 photocatalytic reduction, its presence was checked during the runs, but it was not detected.

Figure 8 reports the comparison among the evolution of CH_4 concentration along irradiation time for TiO_2-PHA, HKUST-1 sample and TiO_2/HKUST-1 hybrid system (during the first and the second test). While a small amount of CH_4 was formed by using the bare samples, a relevant CH_4 production was observed for TiO_2/HKUST-1. For this latter sample, the amount of products obtained during the run carried out after the cleaning procedure, was comparable to those measured during the first run. The higher activity of the hybrid sample suggests the occurrence of a synergistic effect between

RE NPs, which are known to be active in photoreduction reactions, and the MOF grafted onto TiO_2 surface. This finding is in accordance with the XPS, FTIR and TEM results.
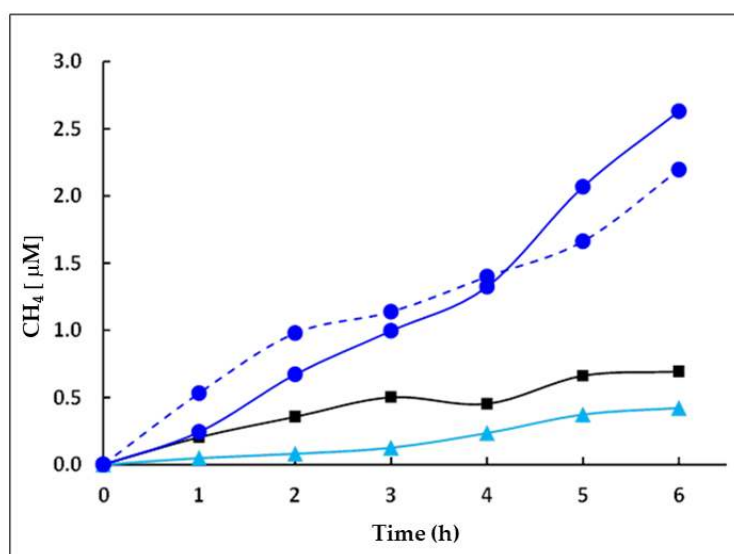

Figure 8. CH_4 evolution in the presence of TiO_2-PHA (black line), HKUST-1 (sky blue line), TiO_2/HKUST-1 first run (dashed blue line) and second run (continuous blue line).

Finally, both the TiO_2 + HKUST-1 sample, obtained by mixing un-functionalized TiO_2 NPs and HKUST-1, and the commercial TiO_2 sample P25, as reference materials, were tested under the same experimental conditions. The TiO_2 + HKUST-1 sample displayed a negligible photoactivity, producing low amounts of CH_4 and CO, in line with the results obtained by using the single components as photocatalysts. This is probably due to: (i) the presence of bare TiO_2 NPs, which are not reactive under solar light; and (ii) the high agglomeration degree of TiO_2 NPs in TiO_2/HKUST-1 may hinder the contact between the catalytic active sites and CO_2 target molecules. In addition, in the presence of commercial TiO_2 P25, we observed only a negligible CH_4 production.

These results support the efficacy of our synthetic approach and highlight the important role of PHA functionalization in order to guarantee a close contact between TiO_2 NPs and MOF, which delivers to TiO_2/HKUST-1 remarkable photoreduction properties.

2.3. Proposed Photocatalytic Pathway

Given the analysis above, a possible mechanism for the enhanced photocatalytic CO_2 reduction over the synthetized TiO_2/HKUST-1 hybrid material was proposed.

To better describe the electronic band structures of TiO_2-PHA NPs and HKUST-1 at the hybrid interface in TiO_2/HKUST-1, the relative energy of the conduction band (CB) and valence band (VB) versus normal hydrogen electrode (NHE) of both pristine HKUST-1 and TiO_2-PHA were calculated, according to Schoonen et al. [70,71], by the empirical equations:

$$E_{CB} = \chi(S) - E^e - 0.5\,E_g \tag{1}$$

$$E_{VB} = E_{CB} + E_g \tag{2}$$

where E_{VB} and E_{CB} are the CB and VB potentials, respectively. Moreover, E_g is the band gap of the semiconductor and E^e is the energy of free electrons vs. hydrogen (~4.5 eV) [72]. Finally, χ is the electronegativity of semiconductor and it was calculated by the following equation:

$$\chi(S) = \sqrt[N]{\chi_1^r\,\chi_2^s\,\cdots\cdots\chi_{n-1}^p\chi_n^q} \tag{3}$$

where χ_n, n, and N are the electronegativity of the constituent atom, the number of species, and the total number of atoms in the compound, respectively [73]. The superscripts r, s, p and q refer to the numbers of the atoms 1, 2, n^{-1}, and n, respectively, in the molecule where $(r + s + \ldots + p + q = N)$.

Although this method cannot give absolute values because the structural factors are neglected, it may provide a rough estimation of the relative energy of CB and VB versus normal hydrogen electrode (NHE).

For HKUST-1, the values of E_g and χ values were 2.7 and 6.17 eV and consequently, E_{CB} and E_{VB} result were 3.02 and 0.32 eV while for TiO_2-PHA E_g and χ were 3.15 and 5.84 eV, and its E_{CB} and E_{VB} as -0.24 and 2.92 eV, respectively, versus NHE, in line with the reported experimental data [74].

With regard to TiO_2-PHA, the presence of the electron trapping sites, associated to Ti(III) sites, as indicated by XPS analysis, was also considered. The energy levels associated to those electron trapping sites could range between 0.1 and 1 eV lower than the anatase CB [75,76].

By considering the values calculated for E_{CB} and E_{VB} of TiO_2-PHA and HKUST-1, a scheme of the energy levels at the TiO_2-PHA/HKUST-1 interface in TiO_2/HKUST-1 can be proposed which suggests a pathway for the CO_2 photoreduction process (Figure 9).
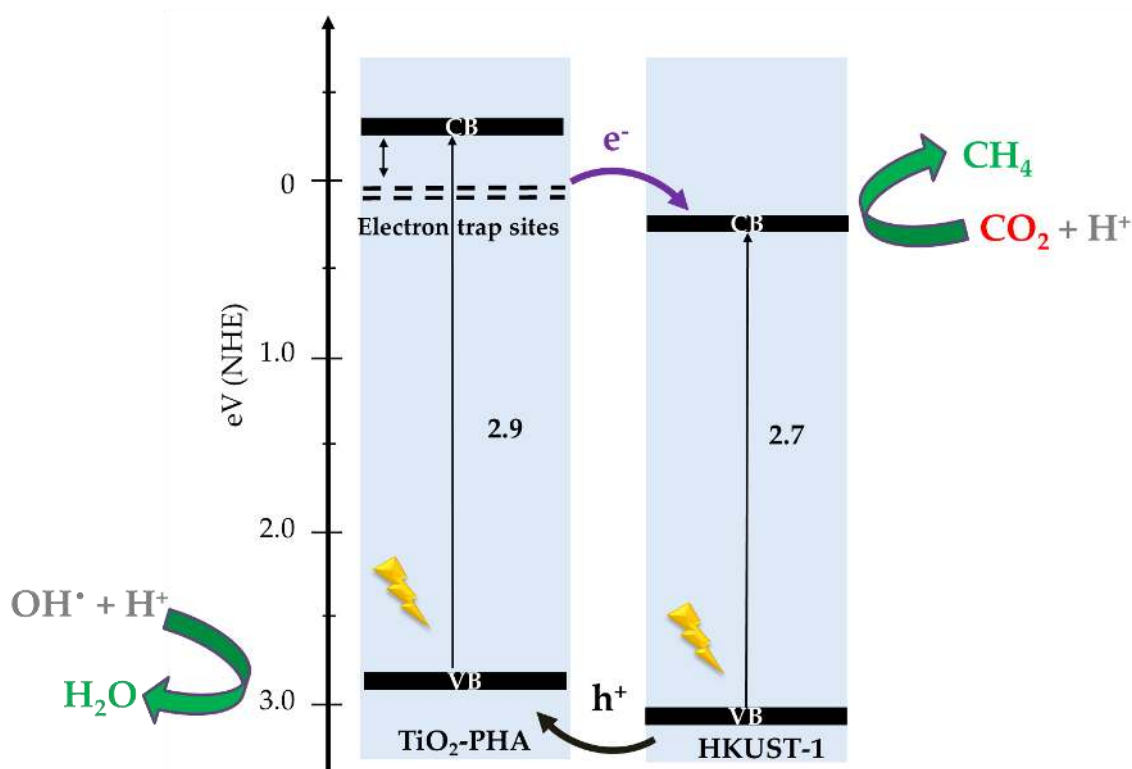

Figure 9. Representative image of the energy levels of TiO_2-PHA and HKUST-1 at the hybrid interface in TiO_2/HKUST-1 with proposed photocatalytic CO_2 photoreduction pathway under sunlight irradiation.

It can be observed that the energy levels of Ti(III) are located at values higher than the CB of HKUST-1. Thus, upon UV-Vis irradiation of TiO_2/HKUST-1, electrons photogenerated from TiO_2-PHA VB can be trapped into Ti(III) centers and easily injected into HKUST-1 CB, thanks to the intimate contact between titania and HKUST-1. This seems to indicate the key role of Ti(III) defective sites of TiO_2-PHA as donor of electrons [77], which can be transferred to HKUST-1 and used in the photocatalytic CO_2 reduction.

Besides, photogenerated holes can migrate toward the VB of TiO_2 and contribute to the water decomposition to OH$\bullet$ and H$^+$ [78]. The whole process highly hinders the electron–hole recombination [79,80], boosting the photoreduction activity of TiO_2/HKUST-1.

Finally, considering the significant amount of copper in TiO_2/HKUST-1, we cannot exclude its involvement in the photocatalytic reaction. Indeed, the beneficial effect of Cu toward the CO_2 photoreduction is well-known [61,64]. In the present case, the improved TiO_2 photoactivity may be connected to the simultaneous presence in TiO_2/HKUST-1 of Cu(II) and Cu(I) species, as revealed by XPS analysis. According to Slamet et al. [81], Cu(II) can be easily reduced by photoexcited electrons to Cu(I), while this latter species, in the presence of H^+ or O_2, can be re-oxidized giving Cu(II) centers and electrons. This redox cycle may also contribute to enhance the photoreduction performance of TiO_2/HKUST-1 hybrid material.

In order to provide a further experimental probe of the suggested mechanism, Electron Spin Resonance (EPR) investigation was tentatively performed on both TiO_2/HKUST-1 hybrid material and TiO_2 + HKUST-1 mixture. The results evidenced the presence of a broad and intense signal related to Cu^{2+} species, which are very abundant in HKUST-1. This feature appears almost unaffected by the irradiation and, due to its intensity and broadness, did not allow to discriminate the possible presence of other resonances (e.g., those related to Ti^{3+} or O^-/$O_2{}^-$ species of titania).

3. Materials and Methods

3.1. Materials

$Ti(OBu)_4$ or TB, 97%, $C_{18}H_{33}CO_2H$ or OA, 90%, $C_{18}H_{35}NH_2$ or OM 70%, TMAH solution 25 wt. % in H_2O, PHA, copper(II) acetate AcCu(II), benzene-1,3,5-tricarboxylic acid (trimesic acid, H_3BTC), ethanol (EtOH) were all purchased from Aldrich and used without further purification.

3.2. Synthesis of Shape-Controlled TiO_2 NPs and Functionalization with PHA

In a typical experiment, TB (44 mmol, 15.0 g) was added to a mixture containing 88 mmol of OA (25.0 g) and 132 mmol (35.3 g) of OM in 25 mL of absolute EtOH. The obtained mixture was stirred for 15 min and then transferred into a 400 mL Teflon-lined stainless-steel autoclave containing 85 mL of absolute EtOH and 3.5 mL of Milli-Q water. The system was then heated at 180 °C and kept at this temperature for 18 h. After decantation, the TiO_2 powder was recovered from the autoclave, washed with EtOH several times, filtered and finally dried in vacuum ($p < 10^{-2}$ mbar) at room temperature. Then, the TiO_2 NPs were dispersed by ultrasound in EtOH solution and then stirred at room temperature for 3 days in the presence of a suitable amount of TMAH (molar ratio TMAH/TiO_2 = 25/1). After decantation, the TiO_2 powder was washed with EtOH several times, filtered and finally dried at 80 °C for 12 h (up to 87% yield).

660 mg of the washed TiO_2 NPs were dispersed by ultrasound in EtOH/water solution (4/1 *v*/*v*) and then functionalized with 540 mg of PHA. The solution was stirred for 24 h at reflux (Scheme 1, STEP 3), then the TiO_2-PHA NPs were collected by centrifugation and the powders were washed several times with EtOH and dried in an oven at 80 °C for 12 h.

3.3. Synthesis of TiO_2/HKUST-1 Hybrid Catalyst

In a typical reaction, a fixed amount of TiO_2-PHA (300 mg) was firstly dispersed and sonicated for 10 min in an EtOH/H_2O 1:1 solution. Simultaneously, two solutions with the precursors AcCu(II) and H_3BTC have been prepared. In the first, 355 mg AcCu(II) were dissolved in 20 mL of EtOH/H_2O 1:1 solution at 45 °C, while 222 mg of H_3BTC were dispersed in 10 mL of EtOH/H_2O to obtain the second solution. After that, the two solutions were mixed with the TiO_2-PHA suspension prepared before. The suspension was stirred for 30 min at 45 °C and then the product was collected by centrifugation and the powders were re-dispersed in the EtOH/H_2O solution. This suspension was mixed again with the AcCu(II) and H_3BTC solutions. The process was repeated three times in order to obtain a material with a higher percentage of MOF. Finally, the TiO_2/HKUST-1 powders obtained were washed 3 times with EtOH/H_2O 1:1 and dried at 80 °C in an oven for one night.

Notably, the photocatalyst was carefully treated to remove possible organic contaminants. To eliminate the solvent and other organic agents from the pores of the TiO_2/HKUST-1 hybrid materials, the powders were treated in vacuum at 150 °C for one night in a Büchi.

In order to highlight the photocatalytic performance of TiO_2/HKUST-1, the following reference materials were also prepared: (i) pristine HKUST-1 and (ii) a composite material constituted of not-functionalized TiO_2 and HKUST-1, obtained by the same procedure described before and labeled as TiO_2+HKUST-1.

3.4. Characterization of TiO_2 NPs, HKUST-1 and TiO_2/HKUST-1

Analyses of the crystalline materials for phase identification were performed by PXRD. PXRD data were collected on a Rigaku Miniflex 600 diffractometer in reflectance Bragg–Brentano geometry with graphite monochromatized Cu-Kα radiation (λ = 1.5406 Å) at 600 W (40 kV, 15 mA) power. Samples were mounted on a zero-background silicon sample holder by dropping powders from a spatula and then gently leveling the sample surface with a razor blade. Samples were not ground before PXRD measurements. Scan rates were 1°/min with 0.02° angular steps in the 2θ range 2–65°. Data were analysed with PDXL2 software (Rigaku, Tokyo, Japan) and Qualx2 [82].

To preliminarily check the TiO_2 washing and PHA functionalization and, successively, the formation of the HKUST-1 structure, ATR-FTIR measurements were performed on a Perkin Elmer Spectrum 100 instrument (1 cm^{-1} resolution spectra, 650–4000 cm^{-1} region, 16 scans).

To quantitatively assess the PHA and MOF grafting onto TiO_2 surfaces, thermogravimetric analysis (TGA) measurements were carried out. TGA thermograms were collected by a Mettler Toledo TGA/DSC1 STARe System, at a constant gas flow (50 cm^3 min^{-1}). The sample powders were heated in air from 30 to 1000 °C. The thermal profile was the following: 30–150 °C at 2 °C min^{-1}; dwell at 150 °C for 120 min; 150–1000 °C at 5 °C min^{-1}.

Morphological characterization by HRTEM and SAED of bare TiO_2 NPs and TiO_2/HKUST-1 powders were performed on a ZEISS LIBRA200FE EFTEM. Elemental composition was evaluated by STEM-EDS analysis (Scanning Transmission Electron Microscopy-Energy Dispersive X-ray Spectrometry Oxford INCA Energy TEM 200, Oxford Instruments, Abingdon-on-Thames, U.K.) of representative grains. The powders were suspended in isopropyl alcohol, sonicated and deposited onto a holey carbon film supported TEM grids. For STEM-EDS analysis holey-carbon molybdenum TEM grids were used. Samples were analyzed after overnight drying.

Low-pressure N_2 adsorption isotherm on HKUST-1 NPs were recorded by a Micromeritics ASAP2020 apparatus. The specific surface area (SSABET, BET method) was measured after evacuation of the samples at 120 °C for 12 h. A liquid N_2 bath was used for measurements at 77 K.

The CO_2 sorption was evaluated at room temperature (293 K) and controlled CO_2 pressure (p$_{CO_2}$ from 5 to 920 mmHg) by Micromeritics ASAP 2020 after evacuation at 120 °C for 12 h.

DR-UV/Vis spectra of carefully ground powders were recorded in the 800–200 nm range with a UV Lambda 900 PerkinElmer spectrophotometer (PerkinElmer, Waltham, MA, USA), equipped with a diffuse reflectance accessory Praying Mantis sampling kit (Harrick Scientific Products, Pleasantville, NY, USA). A Spectralon disk was used as reference material.

The surface chemical composition of the TiO_2, TiO_2-PHA NPs, HKUST-1 and TiO_2/HKUST-1 powders was investigated by XPS. Analysis was performed on the as-prepared powders samples, fixing them on the sample holder using carbon tape. The XPS spectra were acquired in ultrahigh vacuum (base pressure: ~4 × 10^{-10} mbar) at room temperature in normal emission geometry using a conventional Mg X-ray source (hν = 1253.6 eV) and a hemispherical electron energy analyzer (total energy resolution ~0.8 eV). Due to charging effects, all BEs are calibrated by fixing the C 1*s* BE of atmospheric contamination at 284.6 eV [83]. The standard deviation for the BEs values was ~±0.2 eV. Survey scans were obtained in the 0–1100 eV range. Detailed scans were recorded for the O 1*s*, Ti 2*p*, and Cu 2*p* regions. To individuate all the possible differences between the samples, XPS spectra were reproduced by fitting the experimental data using a Shirley background and

several Doniach-Sunjich components [84], corresponding to different oxidation states and chemical environments [85]. The fitting parameters have been fixed following Kaushik [86] and taking into account the energy resolution used in the measurements (~0.8 eV).

The EPR investigation was performed by a Bruker EMX spectrometer operating at the X-band frequency and equipped with an Oxford cryostat. The spectra of TiO_2/HKUST-1 hybrid material and TiO_2 + HKUST-1 mixture were carried out at 130 °C in vacuum conditions ($p < 10^{-5}$ mbar), before and after UV-Vis irradiation, directly inside the EPR cavity.

3.5. Photocatalytic CO_2 Reduction

The photocatalytic CO_2 reduction was carried out in a batch cylindrical gas–solid reactor (V = 120 mL) containing 0.3 g of powder distributed as a thin layer. The system was irradiated from the top with a solar light simulating lamp (1500 W high pressure Xe lamp) inside a SOLARBOX (CO.FO.ME.GRA.). The reaction temperature was 60 °C.

The possible presence of products deriving from C impurities was checked by means of the standardized procedure reported by Mei et al. [69]. In the first step, after prolonged purging with water-saturated He, the photocatalyst was irradiated for about 2 h in contact with Helium in water vapor, (i.e., in the absence of CO_2). Then the system was completely purged again with Helium, to remove all carbon-containing species in the gas phase. The cleaning procedure was repeated until carbon contaminations were removed from the sample surface. After this so-called cleaning step, the photocatalytic tests were performed. In detail, the system was saturated with wet CO_2. 500 μL of the gaseous mixture were withdrawn from the reactor for analyses at fixed irradiation times by using a gas-tight microsyringe. The evolution of CH_4 and CO was followed by a HP 6890 Series GC equipped with a packed column GC 60/80 Carboxen-1000 and a TCD detector, whilst the concentration of the organic species was measured by a GC-2010 Shimadzu gas chromatograph equipped with a Phenomenex Zebron Wax-plus column (30 m × 0.32 μm × 0.53 μm) and a flame ionization detector, using He as the carrier gas. Each photocatalyst was tested three times, to check the reproducibility of the photocatalytic runs, in terms of CO_2 (in the cleaning step), CH_4 and CO production.

4. Conclusions

In summary, a novel hybrid TiO_2/HKUST-1 photocatalyst was successfully obtained via a slow-diffusion method combined with step-by-step self-assembly approach at room temperature, starting from TiO_2 NPs functionalized with an asymmetric organic linker. Our synthetic approach promotes the crystalline growth of MOF layers on titania surface and favors an intimate contact between HKUST-1 and TiO_2-PHA.

The close contact between two hybrid components is a key point for expressing the remarkable performance of the hybrid material. In fact, this allows not only a high CO_2 uptake into the porous MOF structure but also, under solar light irradiation, favors an improved photoreduction activity of TiO_2/HKUST-1 compared to that of pure TiO_2-PHA and HKUST-1 samples.

The remarkable photoreduction ability of the material was related to the improved visible light absorption and to an effective electron injection from TiO_2-PHA to HKUST-1 involving both photogenerated electrons and those trapped in Ti(III) centers of TiO_2-PHA. This indicates that in the hybrid TiO_2/HKUST-1 photocatalyst, also the presence of electrons deriving from a redox active role of TiO_2-PHA can be exploited in the photocatalytic reduction of CO_2. Moreover, the performance of the material was confirmed by subsequent photocatalytic runs carried out with the same sample.

We expect that our synthetic approach will enable the possibility to fabricate a wider range of hybrid porous photocatalytic materials, namely TiO_2/MOF, with a designable MOF shell, suitable for a variety of energy and environmental applications. Particularly, the structure, composition, and function of the MOF shell could also be judiciously tailored by choosing different framework building blocks, i.e., metal ion and polyfunctional organic likers.

Supplementary Materials: The following are available online at http://www.mdpi.com/2073-4344/8/9/353/s1, Table S1: Structural parameters and porosity of RE TiO_2 NPs, Figure S1: TEM micrographs and related SAED analysis of TiO_2 anatase crystals and TiO_2/HKUST-1 hybrid system, Figure S2. STEM-EDS spectra, Figure S3: Kubelka-Munk function of TiO_2-PHA, pure HKUST-1 and TiO_2/HKUST-1, Figure S4: XPS survey spectra of TiO_2, TiO_2-PHA, HKUST-1 and TiO_2/HKUST-1, Figure S5: High resolution XPS spectra of O 1*s* in HKUST-1, TiO_2, TiO_2-PHA and TiO_2/HKUST-1, Table S2: Results of the photocatalytic runs in the presence of the TiO_2-PHA sample, Table S3: Results of the photocatalytic runs in the presence of the bare HKUST-1 sample, Table S4: Results of the photocatalytic runs in the presence of the sample TiO_2/HKUST-1, Figure S6: TEM image and PXRD pattern of TiO_2/HKUST after the second photocatalytic run.

Author Contributions: B.D.C. supervised the project and worked at the preparation of the manuscript; M.R. and E.C. performed the preparation of the catalysts and most of the thermal and spectroscopic characterizations; M.B. carried out the photocatalytic experiments, M.M. (Massimo Moret) the PXRD analysis, M.C. the BET analysis, C.C. the XPS experiments, M.M. (Marcello Marelli)and C.E. the morphological characterization; M.B. and L.P. gave technical support and conceptual advice in photocatalytic measurements. M.D. and R.S. gave conceptual advice for implementing and editing the manuscript. All authors discussed the results and implications and commented on the manuscript at all stages.

Conflicts of Interest: The authors declare no conflict of interest.

References

1. Chang, X.; Wang, T.; Gong, J. CO_2 photo-reduction: Insights into CO_2 activation and reaction on surfaces of photocatalysts. *Energy Environ. Sci.* **2016**, *9*, 2177–2196. [CrossRef]

2. Monastersky, R. Global carbon dioxide levels near worrisome milestone. *Nature* **2013**, *497*, 13–14. [CrossRef] [PubMed]

3. Song, C. Global challenges and strategies for control, conversion and utilization of CO_2 for sustainable development involving energy, catalysis, adsorption and chemical processing. *Catal. Today* **2006**, *115*, 2–32. [CrossRef]

4. Roy, S.C.; Varghese, O.K.; Paulose, M.; Grimes, A.C. Toward solar fuels: Photocatalytic conversion of carbon dioxide to hydrocarbons. *ACS Nano* **2010**, *4*, 1259–1278. [CrossRef] [PubMed]

5. Zhao, G.; Huang, X.; Wang, X.; Wang, X. Progress in catalyst exploration for heterogeneous CO_2 reduction and utilization: A critical review. *J. Mater. Chem. A* **2017**, *5*, 21625–21649. [CrossRef]

6. D'Alessandro, D.M.; Smit, B.; Long, J.R. Carbon dioxide capture: Prospects for new materials. *Angew. Chem. Int. Ed.* **2010**, *49*, 6058–6082. [CrossRef] [PubMed]

7. White, J.L.; Baruch, M.F.; Pander, J.E., III; Hu, Y.; Fortmeyer, I.C.; Park, J.E.; Zhang, T.; Liao, K.; Gu, J.; Yan, Y.; et al. Light-driven heterogeneous reduction of carbon dioxide: Photocatalysts and photoelectrodes. *Chem. Rev.* **2015**, *115*, 12888–12935. [CrossRef] [PubMed]

8. Xu, H.; Ouyang, S.; Liu, L.; Reunchan, P.; Umezawa, N.; Ye, J. Recent advances in TiO_2-based photocatalysis. *J. Mater. Chem. A* **2014**, *2*, 12642–12661. [CrossRef]

9. Ringsmuth, A.K.; Landsberg, M.J.; Hankamer, B. Can photosynthesis enable a global transition from fossil fuels to solar fuels, to mitigate climate change and fuel-supply limitations? *Renew. Sustain. Energy Rev.* **2016**, *62*, 134–163. [CrossRef]

10. Indrakanti, V.P.; Kubicki, J.D.; Schobert, H.H. Photoinduced activation of CO_2 on Ti-based heterogeneous catalysts: Current state, chemical physics-based insights and outlook. *Energy Environ. Sci.* **2009**, *2*, 745–758. [CrossRef]

11. Yu, J.; Low, J.; Xiao, W.; Zhou, P.; Jaroniec, M. Enhanced photocatalytic CO_2-reduction activity of anatase TiO_2 by coexposed {001} and {101} facets. *J. Am. Chem. Soc.* **2014**, *136*, 8839–8842. [CrossRef] [PubMed]

12. Li, K.; Peng, T.; Ying, Z.; Song, S.; Zhang, J. Ag-loading on brookite TiO_2 quasi nanocubes with exposed {210} and {001} facets: Activity and selectivity of CO_2 photoreduction to CO/CH_4. *Appl. Catal. B Environ.* **2016**, *180*, 130–138. [CrossRef]

13. Liu, S.; Yu, J.; Jaroniec, M. Tunable photocatalytic selectivity of hollow TiO_2 microspheres composed of anatase polyhedra with exposed {001} facets. *J. Am. Chem. Soc.* **2010**, *132*, 11914–11916. [CrossRef] [PubMed]

14. Di Credico, B.; Bellobono, I.R.; D'Arienzo, M.; Fumagalli, D.; Redaelli, M.; Scotti, R.; Morazzoni, F. Efficacy of the reactive oxygen species generated by immobilized hydrothermal TiO_2 in the photocatalytic degradation of diclofenac. *Intern. J. Photoenergy* **2015**. [CrossRef]

15. Anandan, S.; Yoon, M. Photocatalytic activities of the nano-sized TiO$_2$-supported Y-zeolites. *J. Photochem. Photobiol. C* **2003**, *4*, 5–18. [CrossRef]

16. Kang, C.; Jing, L.; Guo, T.; Cui, H.; Zhou, J.; Fu, H. Synthesis of high-temperature stable anatase TiO$_2$ photocatalyst. *J. Phys. Chem. C* **2009**, *213*, 1006–1013. [CrossRef]

17. Hu, P.; Morabito, J.V.; Tsung, C.K. Core−shell catalysts of metal nanoparticle core and metal−organic framework shell. *ACS Catal. A* **2014**. [CrossRef]

18. Furukawa, H.; Cordova, K.E.; O'Keeffe, M.; Yaghi, O.M. The chemistry and applications of metal-organic frameworks. *Science* **2013**, *341*, 974–985. [CrossRef] [PubMed]

19. Xuan, W.; Zhu, C.; Liu, Y.; Cui, Y. Mesoporous metal–organic framework materials. *Chem. Soc. Rev.* **2012**, *41*, 1677–1695. [CrossRef] [PubMed]

20. Rossin, A.; Di Credico, B.; Giambastiani, G.; Peruzzini, M.; Pescitelli, G.; Reginato, G.; Borfecchia, E.; Gianolio, G.; Lamberti, C.; Bordiga, S. Synthesis, characterization and CO$_2$ uptake of a chiral Co(II) metal–organic framework containing a thiazolidine-based spacer. *J. Mater. Chem.* **2012**, *22*, 10335–10344. [CrossRef]

21. Rossin, A.; Ienco, A.; Costantino, F.; Montini, T.; Di Credico, B.; Caporali, M.; Gonsalvi, L.; Fornasiero, P.; Peruzzini, M. Phase transitions and CO$_2$ adsorption properties of polymeric magnesium formate. *Cryst. Growth Des.* **2008**, *8*, 3302–3308. [CrossRef]

22. So, M.C.; Wiederrecht, G.P.; Mondloch, J.E.; Hupp, J.T.; Farha, O.K. Metal–organic framework materials for light-harvesting and energy transfer. *Chem. Commun.* **2015**, *51*, 3501–3505. [CrossRef] [PubMed]

23. Yan, S.; Ouyang, S.; Xu, H.; Zhao, M.; Zhang, X.; Ye, J. Co-ZIF-9/TiO$_2$ nanostructure for superior CO$_2$ photoreduction activity. *Mater. Chem. A* **2016**, *4*, 15126–15133. [CrossRef]

24. Crake, A.; Christoforidis, K.C.; Kafizas, A.; Zafeiratos, S.; Petit, C. CO$_2$ capture and photocatalytic reduction using bifunctional TiO$_2$/MOF nanocomposites under UV–vis irradiation. *Appl. Catal. B Environ.* **2017**, *210*, 131–140. [CrossRef]

25. Wang, S.; Wang, X. Multifunctional metal–organic frameworks for photocatalysis. *Small* **2015**, *11*, 3097–3112. [CrossRef] [PubMed]

26. Li, X.; Pi, Y.; Xia, Q.; Li, Z.; Xia, J. TiO$_2$ encapsulated in Salicylaldehyde-NH2-MIL-101(Cr) for enhanced visible light-driven photodegradation of MB. *Appl. Catal. B Environ.* **2016**, *191*, 192–201. [CrossRef]

27. Wang, D.; Huang, R.; Liu, W.; Sun, D.; Li, Z. Fe-based MOFs for photocatalytic CO$_2$ reduction: Role of coordination unsaturated sites and dual excitation pathways. *ACS Catal.* **2014**, *4*, 4254–4260. [CrossRef]

28. Bloch, E.D.; Britt, D.; Lee, C.; Doonan, C.J.; Uribe-Romo, F.J.; Furukawa, H.; Long, J.R.; Yaghi, O.M. Metal insertion in a microporous metal−organic framework lined with 2,2′-bipyridine. *J. Am. Chem. Soc.* **2010**, *132*, 14382–14384. [CrossRef] [PubMed]

29. Sun, D.; Gao, Y.; Fu, J.; Zeng, X.; Chen, Z.; Li, Z. Construction of a supported Ru complex on bifunctional MOF-253 for photocatalytic CO$_2$ reduction under visible light. *Chem. Commun.* **2015**, *51*, 2645–2648. [CrossRef] [PubMed]

30. Shen, L.; Xu, C.; Qi, X.; Cao, Y.; Tang, J.; Zheng, Y.; Jiang, L. Highly efficient Cu$_x$O/TiO$_2$ catalysts: Controllable dispersion and isolation of metal active species. *Dalton Trans.* **2016**, *45*, 4491–4495. [CrossRef] [PubMed]

31. Chui, S.S.Y.; Lo, S.M.F.; Charmant, J.P.H.; Orpen, A.G.; Williams, I.D. Chemically functionalizable nanoporous material [Cu$_3$(TMA)$_2$(H$_2$O)$_3$]$_n$. *Science* **1999**, *283*, 1148–1150. [CrossRef] [PubMed]

32. Millward, A.R.; Yaghi, O.M. Metal−organic frameworks with exceptionally high capacity for storage of carbon dioxide at room temperature. *J. Am. Chem. Soc.* **2005**, *127*, 17998–17999. [CrossRef] [PubMed]

33. Wang, Q.M.; Shen, D.; Bulow, M.; Lau, M.L.; Deng, S.; Fitch, F.R.; OLemcoff, N.; Semanscin, J. Metallo-organic molecular sieve for gas separation and purification. *Micropor. Mesopor. Mater.* **2002**, *55*, 217–230. [CrossRef]

34. Schlichte, K.; Kratzke, T.; Kaskel, S. Improved synthesis, thermal stability and catalytic properties of the metal-organic framework compound Cu$_3$(BTC)$_2$. *Micropor. Mesopor. Mater.* **2004**, *3*, 81–88. [CrossRef]

35. Alaerts, L.; Seguin, E.; Poelman, H.; Thibault-Starzyk, F.; Jacobs, P.A.; De Vos, D.E. Probing the Lewis acidity and catalytic activity of the metal-organic framework [Cu$_3$(BTC)$_2$] (BTC = benzene-1,3,5-tricarboxylate). *Chem. Eur. J.* **2006**, *12*, 7353–7363. [CrossRef] [PubMed]

36. Li, R.; Hu, J.; Deng, M.; Wang, H.; Wang, X.; Hu, Y.; Jiang, H.L.; Jiang, J.; Zhang, Q.; Xie, Y.; et al. Integration of an Inorganic Semiconductor with a Metal–Organic Framework: A Platform for Enhanced Gaseous Photocatalytic Reactions. *Adv. Mater.* **2014**, *26*, 4783–4788. [CrossRef] [PubMed]

37. He, X.; Gan, Z.; Fisenko, S.; Wang, D.; El-Kaderi, H.M.; Wang, W.-N. Rapid formation of metal−organic frameworks (MOFs) based nanocomposites in microdroplets and their applications for CO_2 photoreduction. *ACS Appl. Mater. Interfaces* **2017**, *9*, 9688–9698. [CrossRef] [PubMed]

38. Anpo, M.; Thomas, J.M. Single site photocatalytic solids for the decomposition of undesirable molecules. *Chem. Commun.* **2006**, *21*, 3273–3278. [CrossRef] [PubMed]

39. Ke, F.; Yuan, Y.P.; Qiu, L.G.; Shen, Y.H.; Xie, A.J.; Zhu, J.F.; Tianc, X.Y.; Zhang, L.D. Facile fabrication of magnetic metal–organic framework nanocomposites for potential targeted drug delivery. *J. Mater. Chem.* **2011**, *21*, 3843–3848. [CrossRef]

40. Anpo, M.; Yamashita, H.; Ichihashi, Y.; Ehara, S. Photocatalytic reduction of CO_2 with H_2O on various titanium oxide catalysts. *J. Electroanal. Chem.* **1995**, *396*, 21–26. [CrossRef]

41. D'Arienzo, M.; Dozzi, M.V.; Redaelli, M.; Di Credico, B.; Morazzoni, F.; Scotti, R.; Polizzi, S. crystal surfaces and fate of photogenerated defects in shape controlled anatase nanocrystals: Drawing useful relations to improve the H_2 yield in methanol photosteam reforming. *J. Phys. Chem. C* **2015**, *119*, 12385–12393. [CrossRef]

42. Ke, F.; Qiu, L.G.; Yuan, Y.P.; Jiang, X.; Zhu, J.F. Fe_3O_4@MOF core-shell magnetic microspheres with a designable metal–organic framework shell. *J. Mater. Chem.* **2012**, *22*, 9497–9500. [CrossRef]

43. D'Arienzo, M.; Carbajo, J.; Bahamonde, A.; Crippa, M.; Polizzi, S.; Scotti, R.; Wahba, L.; Morazzoni, F. Photogenerated defects in shape-controlled TiO_2 anatase nanocrystals: A probe to evaluate the role of crystal facets in photocatalytic processes. *J. Am. Chem. Soc.* **2011**, *133*, 17652–17661. [CrossRef] [PubMed]

44. Liu, Y.; Tang, A.; Zhang, Q.; Yin, Y. Seed-mediated growth of anatase tio2 nanocrystals with core-antenna structures for enhanced photocatalytic activity. *J. Am. Chem. Soc.* **2015**, *137*, 11327–11339. [CrossRef] [PubMed]

45. Horn, M.; Schwerdtfeger, C.F.; Meagher, E.P. Refinement of the structure of anatase at several temperatures. *Zeitschrift fuer Kristallographie* **1972**, *136*, 273–281. [CrossRef]

46. Summerfield, A.; Cebula, I.; Schröder, M.; Beton, P.H. Nucleation and early stages of layer-by-layer growth of metal organic frameworks on surfaces. *J. Phys. Chem. C* **2015**, *119*, 23544–23551. [CrossRef] [PubMed]

47. Cubillas, P.; Anderson, M.W. Synthesis mechanism: Crystal growth and nucleation. In *Zeolites and Catalysis: Synthesis, Reactions and Applications*; Wiley-VCH Verlag GmbH & Co. KGaA: Weinheim, Germany, 2010.

48. Guerrero, G.; Mutin, P.H.; Vioux, A. Anchoring of phosphonate and phosphinate coupling molecules on titania particles. *Chem. Mater.* **2001**, *13*, 4367–4373. [CrossRef]

49. Prestipino, C.; Regli, L.; Vitillo, J.G.; Bonino, F.; Damin, A.; Lamberti, C.; Zecchina, A.; Solari, P.L.; Kongshaug, K.O.; Bordiga, S. Local structure of framework Cu(II) in HKUST-1 metallorganic framework: Spectroscopic characterization upon activation and interaction with adsorbates. *Chem. Mater.* **2006**, *18*, 1337–1346. [CrossRef]

50. Dinh, C.T.; Nguyen, T.D.; Kleitz, F.; Do, T.O. Shape-controlled synthesis of highly crystalline titania nanocrystals. *ACS Nano* **2009**, *3*, 3737–3743. [CrossRef] [PubMed]

51. Thommes, M.; Cychosz, K.A. Physical adsorption characterization of nanoporous materials: Progress and challenges. *Adsorption* **2014**, *20*, 233–250. [CrossRef]

52. Yan, X.; Komarneni, S.; Zhang, Z.; Yan, Z. Extremely enhanced CO_2 uptake by HKUST-1 metal-organic frameworks via a simple chemical treatment. *Micropor. Mesopor. Mater.* **2014**, *183*, 69–73. [CrossRef]

53. Wong-Foy, A.G.; Lebel, O.; Matzger, A.J. Porous crystal derived from a tricarboxylate linker with two distinct binding motifs. *J. Am. Chem. Soc.* **2007**, *129*, 15740–15741. [CrossRef] [PubMed]

54. Kim, T.K.; Suh, M.P. Selective CO_2 adsorption in a flexible non-interpenetrated metal-organic framework. *Chem. Commun.* **2011**, *47*, 4258–4260. [CrossRef] [PubMed]

55. Chen, Z.; Xiang, S.; Arman, H.D.; Li, P.; Tidrow, S.; Zhao, D.; Chen, B. Microporous metal–organic framework with immobilized–oh functional groups within the pore surfaces for selective gas sorption. *Eur. J. Inorg. Chem.* **2010**. [CrossRef]

56. Shekhah, O.; Liu, J.; Fischer, R.A.; Woll, C. MOF thin films: Existing and future applications. *Chem. Soc. Rev.* **2011**, *40*, 1081–1086. [CrossRef] [PubMed]

57. Zhang, Y.G.; Ma, L.L.; Li, J.L.; Yu, Y. In situ Fenton reagent generated from TiO_2/Cu_2O composite film: A new way to utilize TiO_2 under visible light irradiation. *Environ. Sci. Technol.* **2007**, *41*, 6264–6269. [CrossRef] [PubMed]

58. Kong, M.; Li, Y.; Chen, X.; Tian, T.; Fang, P.; Zheng, F.; Zhao, X. Tuning the relative concentration ratio of bulk defects to surface defects in TiO_2 nanocrystals leads to high photocatalytic efficiency. *J. Am. Chem. Soc.* **2011**, *133*, 16414–16417. [CrossRef] [PubMed]

59. Liu, X.; Xu, H.; Grabstanowicz, L.; Gao, S.; Lou, Z.; Wang, W.; Huang, B.; Dai, Y.; Xu, T. Ti^{3+} self-doped TiO_{2-x} anatase nanoparticles via oxidation of TiH_2 in H_2O_2. *Catal. Today* **2014**, *225*, 80–89. [CrossRef]

60. Abate, A.; Pérez-Tejada, R.; Wojciechowski, K.; Foster, J.M.; Sadhanala, A.; Steiner, U.; Snaith, H.J.; Franco, S.; Ordunac, J. Phosphonic anchoring groups in organic dyes for solid-state solar cells. *Phys. Chem. Chem. Phys.* **2015**, *17*, 18780–18789. [CrossRef] [PubMed]

61. Bellardita, M.; Di Paola, A.; García-López, E.; Loddo, V.; Marcì, G.; Palmisano, L. Photocatalytic CO_2 reduction in gas-solid regime in the presence of bare, SiO_2 supported or Cu-loaded TiO_2 samples. *Curr. Org. Chem.* **2013**, *17*, 2440–2448. [CrossRef]

62. Marcì, G.; García-López, E.I.; Palmisano, L. Photocatalytic CO_2 reduction in gas–solid regime in the presence of H_2O by using GaP/TiO_2 composite as photocatalyst under simulated solar light. *Catal. Commun.* **2014**, *53*, 38–41. [CrossRef]

63. Zhao, C.; Liu, L.; Zhang, Q.; Wang, J.; Li, Y. Photocatalytic conversion of CO_2 and H_2O to fuels by nanostructured $Ce–TiO_2/SBA-15$ composites. *Catal. Sci. Technol.* **2012**, *2*, 2558–2568. [CrossRef]

64. Liu, D.; Fernández, Y.; Ola, O.; Mackintosh, S.; Maroto-Valer, M.; Parlett, C.M.A.; Lee, A.F.; Wu, J.C.S. On the impact of Cu dispersion on CO_2 photoreduction over Cu/TiO_2. *Catal. Commun.* **2012**, *25*, 78–82. [CrossRef]

65. Tseng, I.H.; Chang, W.C.; Wu, J.C.S. Photoreduction of CO_2 using sol–gel derived titania and titania-supported copper catalysts. *Appl. Catal. B Environ.* **2002**, *37*, 37–48. [CrossRef]

66. Sellaro, M.; Bellardita, M.; Brunetti, A.; Fontananova, E.; Palmisano, L.; Drioli, E.; Barbieri, G. CO_2 conversion in a photocatalytic continuous membrane reactor. *RSC Adv.* **2016**, *6*, 67418–67427. [CrossRef]

67. Mele, G.; Annese, C.; D'Accolti, L.; De Riccardis, A.; Fusco, C.; Palmisano, L.; Scarlino, A.; Vasapollo, G. Photoreduction of carbon dioxide to formic acid in aqueous suspension: A comparison between phthalocyanine/TiO_2 and porphyrin/TiO_2 catalysed processes. *Molecules* **2015**, *20*, 396–415. [CrossRef] [PubMed]

68. Li, Y.; Wang, W.N.; Zhan, Z.; Woo, M.H.; Wu, C.Y.; Biswas, P. Photocatalytic reduction of CO_2 with H_2O on mesoporous silica supported Cu/TiO_2 catalyst. *Appl. Catal. B Environ.* **2010**, *100*, 386–392. [CrossRef]

69. Mei, B.; Pougin, A.; Strunk, J. Influence of photodeposited gold nanoparticles on the photocatalytic activity of titanate species in the reduction of CO_2 to hydrocarbons. *J. Catal.* **2013**, *306*, 184–189. [CrossRef]

70. Mousavi, M.; Habibi-Yangjeh, A.; Abitorabi, M. Fabrication of novel magnetically separable nanocomposites using graphitic carbon nitride, silver phosphate and silver chloride and their applications in photocatalytic removal of different pollutants using visible-light irradiation. *J. Colloid Interface Sci.* **2016**, *480*, 218–231. [CrossRef] [PubMed]

71. Xu, Y.; Schoonen, M.A.A. The absolute energy positions of conduction and valence bands of selected semiconducting minerals. *Am. Mineral.* **2000**, *85*, 543–556. [CrossRef]

72. Morrison, S.R. *Electrochemistry at Semiconductor and Oxidized Metal Electrode*; Plenum Press: New York, NY, USA, 1980.

73. Sanderson, R.T. *Chemical Periodicity*; Reinhold Pub. Corp.: New York, NY, USA, 1960.

74. Serpone, N.; Pelizzetti, E. *Photocatalysis, Fundamentals and Applications*; Wiley: New York, NY, USA, 1989.

75. Ikeda, S.; Sugiyama, N.; Muratami, S.; Kominami, H.; Kera, Y.; Noguchi, H.; Uosaki, K.; Torimoto, T.; Ohtani, B. Quantitative analysis of defective sites in titanium(IV) oxide photocatalyst powders. *Phys. Chem. Chem. Phys.* **2003**, *5*, 778–783. [CrossRef]

76. Leytner, S.; Hupp, J.T. Evaluation of the energetics of electron trap states at the nanocrystalline titanium dioxide/aqueous solution interface via time-resolved photoacoustic spectroscopy. *Chem. Phys. Lett.* **2000**, *330*, 231–236. [CrossRef]

77. Abdellah, M.; El-Zohry, A.M.; Antila, L.J.; Windle, C.D.; Reisner, E.; Hammarström, L. Time-resolved IR spectroscopy reveals a mechanism with TiO_2 as a reversible electron acceptor in a TiO_2−re catalyst system for CO_2 photoreduction. *J. Am. Chem. Soc.* **2017**, *139*, 1226–1232. [CrossRef] [PubMed]

78. Tan, S.S.; Zou, L.; Hu, E. Photocatalytic reduction of carbon dioxide into gaseous hydrocarbon using TiO_2 pellets. *Catal. Today* **2006**, *115*, 269–273. [CrossRef]

79. Zhang, Q.; Rao, G.; Rogers, J.; Zhao, C.; Liu, L.; Li, Y. Novel anti-fouling Fe_2O_3/TiO_2 nanowire membranes for humic acid removal from water. *Chem. Eng. J.* **2015**, *271*, 180–187. [CrossRef]

80. Hurum, D.C.; Agrios, A.G.; Gray, K.A.; Rajh, T.; Thurnauer, M.C. Explaining the enhanced photocatalytic activity of Degussa P25 mixed-phase TiO_2 using EPR. *J. Phys. Chem. B* **2003**, *107*, 4545–4549. [CrossRef]

81. Slamet, H.W.N.; Ezza, P.; Kapti, R.; Jarnuzi, G. Effect of copper species in a photocatalytic synthesis of methanol from carbon dioxide over copper-doped titania catalysts. *World Appl. Sci. J.* **2009**, *6*, 112–122.

82. Altomare, A.; Corriero, N.; Cuocci, C.; Falcicchio, A.; Moliterni, A.; Rizzi, R. QUALX2.0: A qualitative phase analysis software using the freely available database POW_COD. *J. Appl. Cryst.* **2015**, *48*, 598–603. [CrossRef]

83. Briggs, D.; Seah, M.P. *Practical Surface Analysis by Auger and X-ray Photoelectron Spectroscopy*; John Wiley and Sons Ltd.: Chichester, UK, 1983.

84. Shirley, D.A. High-resolution X-Ray photoemission spectrum of the valence bands of gold. *Phys. Rev. B Condens. Matter* **1972**, *5*, 4709–4714. [CrossRef]

85. Biesinger, M.C.; Payne, B.P.; Grosvenor, A.P.; Lauac, L.W.M.; Gerson, A.R.; Smart, R.S.C. Resolving surface chemical states in XPS analysis of first row transition metals, oxides and hydroxides: Cr, Mn, Fe, Co and Ni. *Appl. Surf. Sci.* **2010**, *257*, 887–898. [CrossRef]

86. Kaushik, V.K. Identification of oxidation states of copper in mixed oxides and chlorides using ESCA[1]. *Spectrochim. Acta Part B* **1989**, *44*, 581–587. [CrossRef]